Mass and occupation fraction of dark matter halos hosting Lyman-α emitters at $z \sim 3$

Jaime E. Forero-Romero[1] and Julian E. Mejía-Restrepo[2]

[1] *Departamento de Física, Universidad de los Andes, Cra. 1 No. 18A-10, Edificio Ip, Bogotá, Colombia*
[2] *Departamento de Astronomía, Universidad de Chile, Camino el Observatorio 1515, Santiago, Chile*

2 January 2014

ABSTRACT
We derive constraints on the mass and occupation fraction of dark matter halos hosting Lyα Emitting galaxies (LAEs) at a redshift of $z = 3.1$ by matching the number density and the angular correlation function between mock and observed fields. We explicitly take into account the cosmic variance on the typical observed field size by constructing mock fields from a large cosmological N-body simulation matching the geometries of observed fields. To populate the halos in the simulation we use a model where a dark matter halo with mass in the range $M_{\min} < M_{\rm h} < M_{\max}$ can only host one detectable LAE with a probability $f_{\rm occ}$. The main motivation to build such a model is to avoid the large uncertainties in the estimation of Lyα luminosities. Our main result is that the clustering and number density information are insufficient to impose a tight constraint on the **occupation** fraction. On the other hand the minimum mass and maximum mass can be tightly constrained to the range $M_{\max} < 10^{12} h^{-1} {\rm M_\odot}$ and $10^{10} h^{-1} {\rm M_\odot} \leq M_{\min} \leq 10^{11.5} h^{-1} {\rm M_\odot}$. We also find that the consistent models have a narrow mass range $\Delta M \equiv \log_{10} M_{\max} - \log_{10} M_{\min}$ smaller than 1.0 dex, with the vast majority in the range $\Delta M < 0.5$ dex. Already published constraints on the mass range and occupation fraction are a sub-set of the models we report in this paper . Our results present an inconclusive response as to which is the occupation fraction for LAEs at $z = 3.1$. A precise answer requires observations on larger fields and robust physical models for the connection between dark matter, star formation and the escape of Lyα radiation. That kind of modeling should also be able to provide a plausible explanation for the narrow range in mass $\Delta M < 1.0$ dex derived here for the halos hosting LAEs at $z = 3.1$.

Key words: cosmology: theory cosmology: large-scale structure of universe galaxies: formation galaxies: high-redshift galaxies: statistics galaxy: haloes

1 INTRODUCTION

Lyman-α emitting galaxies (LAEs) are helpful in a diverse range of subjects in extragalactic astronomy. LAEs can be used as probes of reionization (Dijkstra et al. 2011), tracers of large scale structure (Koehler et al. 2007), signposts for low metallicity stellar populations, markers of the galaxy formation process at high redshift (Dayal et al. 2009; Forero-Romero et al. 2012) and tracers of active star formation (Guaita et al. 2013).

Capitalizing LAEs observations requires an understanding of their place in the context of a given structure formation model in a cosmological context. Under the current paradigm the dominant matter content of the Universe is to be found in dark matter (DM) and each galaxy is thought to be hosted by larger dark matter structure known as a halo. (Peebles 1980; Springel et al. 2005).

Galaxy formation models find that halo mass predicts with high accuracy galactic properties such as stellar mass and star formation rate (Behroozi et al. 2013b). This suggests that the physical processes that regulate the star formation cycle are dependent on halo mass. For that reason, finding the typical dark matter halo mass hosting LAEs represents an advance to understand the nature of this galaxy population in the context of Lambda Cold Dark Matter (ΛCDM) paradigm.

Some theoretical attempts to solve this problem using an ab-initio approach. They start from the DM halo population to infer the intrinsic star formation rates and Lyα a luminosities. From these values they estimate the amount of Lyα photons that escape each galaxy and compute the observed luminosity for each galaxy. These models can predict different observables including: the luminosity function,

correlation function and the equivalent width distributions. Such modelling has been implemented in semi-analytic models (Garel et al. 2012; Orsi et al. 2012; Walker-Soler et al. 2012) and full N-body hydrodynamical simulations (Laursen & Sommer-Larsen 2007; Dayal et al. 2009; Forero-Romero et al. 2011; Yajima et al. 2012).

These calculations involve many uncertain steps, such as the treatment of astrophysical processes describing star formation. However, in the context of LAEs, the dominant uncertainty is the estimation of the escape fraction, that is the fraction of Lyα photons that escape the galaxy to the observer. Given the resonant nature of the Lyα line, the escape fraction is sensitive to the dust contents, density, temperature, topology and kinematics of the neutral Hydrogen in the interstellar medium (ISM). Solving the radiative transfer of Lyα photons in the ISM requires Monte Carlo simulations. The process of finding a consensus on the expected value for the Lyα escape fraction in high redshift galaxies is still matter of ongoing research (Neufeld 1991; Verhamme et al. 2006; Forero-Romero et al. 2011; Dijkstra & Kramer 2012; Laursen et al. 2013; Orsi et al. 2012).

A different approach to infer the typical mass of halos hosting LAEs is based on the spatial clustering information. This approach uses the fact that in CDM cosmologies the spatial clustering of galaxies on large scales is entirely dictated by the halo distribution (Colberg et al. 2000), which in turn has a strong dependence on halo mass. Using measurements of the angular correlation function of LAEs, observers have put constraints on the typical mass and occupation fraction of the putative halos hosting these galaxies (Hayashino et al. 2004; Gawiser et al. 2007; Nilsson et al. 2007; Ouchi et al. 2010). In these studies the observations are done on fields of ~ 1 deg^2 and the conclusions derived on the halo host mass do not delve too deeply into the possible impact of cosmic variance.

Recently Yamada et al. (2012) observed a wide area of 2.4 deg^2 under homogeneous instrumental and data reduction conditions. This data set is constructed from 12 different sub-fields that allows us to use clustering statistics and cosmic variance to constraint the mass and occupation fraction of halos hosting LAEs.

Our method first populates DM halos in cosmological simulations with LAEs. We only consider whether a DM can host a detectable LAE or not without predicting a Lyα luminosity. This bypasses all the physical uncertainties involved in the estimation of observed Lyα luminosities. Once we have the mock LAE catalogs, we compare them against observations in terms of the statistics on the number density distribution derived from the observations over the 12 fields of Yamada et al. (2012). We also use measurements of the angular correlation function to improve these constraints. This method allows us to constraint the preferred mass range and occupation fraction of DM halos hosting LAEs.

This paper is structured as follows. In the next section we present the simulation and the model used to produce the mock catalogs. We also list the criteria used to compare the mocks against observations. In §3 we present the main results for the halo mass and occupation fraction. We continue with a discussion of these results under the light of other observational and theoretical results. Finally, we present our conclusions in §5.

Throughout this paper we assume a ΛCDM cosmology

with the following values for the cosmological parameters, $\Omega_m = 0.27$, $\Omega_\Lambda = 0.73$ and $h = 0.70$, corresponding to the matter density, vacuum density and the Hubble constant in units of 100 km s^{-1} Mpc^{-1}.

2 METHODOLOGY

Our method is based on the comparison of observations and mock catalogs. We use two different kinds of statistics to perform the comparison: (i) the distribution of the surface number density across fields and (ii) the angular correlation function.

In the next subsections we describe in detail the four key elements int our work-flow. First we present (in two subsections) the observations we take as a benchmark. Second, we describe the main characteristics of the N-body simulation and the halo catalogs we use. Third, we recount the important parameters of the simplified model that we use to populate the halo catalogs with LAEs. Finally, we describe some of the statistical tests we adopt to compare observations and mocks .

2.1 Observational constraints

The primary observational constraint we use in this paper is the LAE number density information at $z = 3.1$ obtained by the panoramic narrow-band survey presented by Yamada et al. (2012) from a survey conducted with the Subaru 8.2m telescope and the Subaru Prime Focus Camera, which has a field of view covering 34×27 arc-min, corresponding to a comoving scale of 46×35 Mpc h^{-1} at $z = 3.09$. The narrow band filter used in the survey is centered at 4977 Å with 77 Å width, corresponding to the redshift range $z = 3.062$-3.125 and 41 h^{-1}Mpc comoving scale for the detection of the Lyman-α line centered at $z = 3.09$. The authors reported a total 2161 LAEs with an observed equivalent width, in the observer frame, larger than 190 Å over a total survey area of 2.42 deg^2 that includes 12 sub-fields, this corresponds to average surface number density of 0.24 ± 0.01 arcmin^{-2}.

The survey covered four independent fields:

(i) The first is the SSA22 field of 1.38 deg^2 with 1394 detected LAEs (7 sub-fields), this field has been known to harbor a region with a large density excess of galaxies. **The first sub-field of is taken around the same region observed in Hayashino et al. (2004).**

(ii) The second observed region is composed by the fields Subaru/*XMM-Newton* Deep Survey (SXDS)-North, -Center and -South, with a total of 0.58 deg^2 and 386 LAEs (3 sub-fields).

(iii) The third field is the Subaru Deep Field (SDF) with 0.22 deg^2 and 196 LAEs (1 sub-field), and

(iv) The fourth one is the field around the Great Observatory Optical Deep Survey (GOODS-N) with 0.24 deg^2 and 185 LAEs (1 sub-field).

There is abundant observational work done on LAEs at redshift $z = 3.1$ (Kudritzki et al. 2000; Matsuda et al. 2005; Gawiser et al. 2007; Nilsson et al. 2007; Ouchi et al. 2008a). However, we decide to focus on the data from Yamada et al. (2012) because it has the largest covered area with homogeneous instrumentation conditions (telescope, narrow band
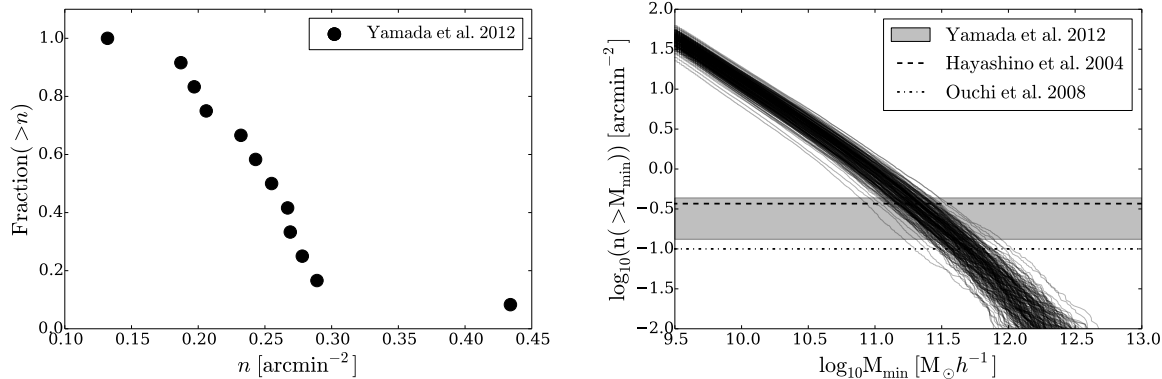
Figure 1. Left panel. Distribution of LAE number densities in all the fields observed by Yamada et al. (2012). The point with the highest surface density corresponds to the densest sub-field in the SSA22 field. Right panel. Surface density of dark matter halos as a function of a minimum halo mass to count the total number of elements in a volume. Each line represents one of the 210 volumes of dimensions $46 \times 35 \times 41 \ h^{-3}$ Mpc^3 in the Bolshoi simulation. The horizontal gray band represents the range of surface densities observed for LAEs at $z = 3.1$ as reported by (Yamada et al. 2012).

filter), data reduction pipeline and conditions to construct the LAE catalog. This ensures that the number density variations among fields are *not* due to different observational conditions or criteria to construct the catalogs.

A secondary benchmark is the angular correlation function (ACF). Yamada et al. (2012) does not report an ACF measurement for their fields. Instead we use the results by Ouchi et al. (2008a) who reported the ACF is over a region of 1 deg^2 over the SXDS field. We also keep track of the results by Hayashino et al. (2004) who reported the ACF in the SSA22 region, including its densest sub-field.

There are some differences between Ouchi et al. (2008a) observations and those by Yamada et al. (2012). The details in the color selection, corresponding limiting luminosities and EW thresholds are different in these references. The average LAEs number density inferred by Hayashino et al. (2004) is 0.37 arcmin^{-2}, which is 30% higher than the new measurement by Yamada et al. (2012). In the case of Ouchi et al. (2008a) the number density is 0.10 arcmin^{-2}, which is $\sim 50\%$ lower than the value inferred by Yamada et al. (2012) for a portion of the same region.

2.2 The adequacy of including SSA22 as an observational benchmark

The field SSA22 has been known to harbor a significant galaxy overdensity. Yamada et al. (2012) estimates that the densest sub-field is likely to be a rare density peak with $3 - 4\sigma$ significance on the scale of $\sim 60 h^{-1}$**Mpc** .

All the other sub-fields in SSA22 are average. They have a similar number density as other blank fields. The left panel in Figure 1 shows the integrated distribution of LAEs number density in all the fields reported in Yamada et al. (2012). It is evident that there is only one sub-field that stands out as an outlier in the distribution (it corresponds to

the densest field in SSA22). All the other fields form a continuous distribution in number density.

Therefore, using the whole SSA22 region as a benchmark in the number density distribution does not impose any bias. However, on has to keep in mind that is not plausible that the full number density distribution from a simulation will include a very dense field. We do not require the presence of such field to judge a mock distribution as successful. The statistical test we perform to compare mock distributions against observations does not require such a perfect match.

In terms of the ACF the results that include the densest field in SSA22 (Hayashino et al. 2004) are consistent, within uncertainties, with the results of other fields (Ouchi et al. 2008a). In spite of this consistency we will focus on the results from (Ouchi et al. 2008a).

2.3 Simulation and halo catalogs

The Bolshoi simulation (Klypin et al. 2011) we use in this paper was performed in a cubic volume of $250 \ h^{-1}$ Mpc on a side. The dark matter distribution is sampled using 2048^3 particles, which translates into a particle mass of $m_{\rm p} = 1.35 \times 10^8 \ h^{-1}$ M$_\odot$. The cosmological parameters are consistent with a WMAP5 and WMAP7 data with a matter density $\Omega_{\rm m} = 0.27$, cosmological constant $\Omega_\Lambda = 0.73$, dimensionless Hubble constant $h = 0.70$, slope of the power spectrum $n = 0.95$ and normalization of the power spectrum$\sigma_8 = 0.82$ (Komatsu et al. 2009; Jarosik et al. 2011).

We use halo catalogs constructed with a Friend-of-Friends (FOF) algorithm with a linking length of 0.17 times the inter-particle distance. The catalogs were obtained from the publicly available Multidark database [1] (Riebe et al. 2013). For each halo in the box we store its comoving position in the box (3-D coordinates) and FOF mass. We focus

---

[1] http://www.multidark.org/MultiDark/

our work on halos more massive than $1 \times 10^{10} h^{-1} \mathrm{M}_\odot$ that are resolved with at least 70 particles, the reasons for this choice are explained in the next sub-section.

2.4   A model to populate halos with LAEs

We assume that a dark matter halo can only host one detectable LAE at most. There are three parameters that decide whether a halo host a LAE: the lower and upper bounds for the mass range, $M_{\mathrm{min}} < M_{\mathrm{h}} < M_{\mathrm{max}}$, where LAEs reside and the fraction f_{occ} of such halos that host a detectable LAE. The reader must keep in mind that the physical interpretation of the occupation fraction f_{occ} convolves two phenomena: the actual presence of a star forming galaxy in a halo and its detectability as a LAE.

We recall that we do not perform a explicit modeling for LAE detectability. Our model does not assign a luminosity or escape fraction for each LAE. We are interested in constraining the halo mass range hosting detectable LAEs commonly used in photometric narrow-band surveys. We also want to explore a wide range of possible masses for the host halos without any strong theoretical prejudice regarding the details of star formation in high-redshift galaxies.

In what follows we note by the letter $\mathcal{M}$ a model defined by a particular choice of the three scalar parameters M_{min}, M_{max} and f_{occ}. For each model $\mathcal{M}$ we create a set of mock fields from disjoint volumes in the simulation. Each volume has the same geometry probed by Suprime-CAM and the narrow band filter, namely rectangular cuboids of dimensions $46 \times 35 \times 41 \ h^{-3} \ \mathrm{Mpc}^3$ where the last dimension goes in the redshift direction. This corresponds to a total area of 880 arcmin^2 in each mock field. We construct a total $5 \times 7 \times 6 = 210$ of such volumes from a snapshot in the Bolshoi simulation. In each mock field a LAE is assigned to the position of a dark matter halo if the halo mass is in the range allowed by the model $M_{\mathrm{min}} < M_{\mathrm{h}} < M_{\mathrm{max}}$ and a random variable taken from an homogeneous distribution $0 \leq \xi < 1$ is smaller than the occupation fraction $\xi < f_{\mathrm{occ}}$.

Next we construct mock surveys by making groups of 12 mock fields out of the 210 available volumes. In total 15 mock surveys are constructed for each model $\mathcal{M}$. The grouping of the 12 mock fields into a mock catalog is done in two different ways. The first is called `match`, it follows the clustering of the observational fields. From the 12 mock fields, 7 are constructed from contiguous fields in the simulation to mimic the SSA22 region, 3 are also contiguous between them but not to the first 7 fields to mimic the SXDS fields and finally 2 non-contiguous fields to imitate the SDF and GOODS-North field. The second way to group the mock fields is called `random`, whereby all the 12 fields are selected in such a way as to avoid that any two volumes are contiguous. In this paper we only report the results obtained by the `match` method and mention explicitly differences observed with the `random` selection.

Figure 2 shows the spatial distribution for one mock survey constructed using the `match` method. Each field corresponds to one of the observational fields. The model parameters to build the mock are $M_{\mathrm{min}} = 10^{10.4} h^{-1} \mathrm{M}_\odot$, $M_{\mathrm{max}} = 10^{0.5} h^{-1} \mathrm{M}_\odot$ and $f_{\mathrm{occ}} = 0.1$. The figure shows only one out of the 15 different mock surveys that are constructed

for each model. We note that we only use $15 \times 12 = 180$ mock fields out of the total of 210 available sub-volumes. The reason is that the `match` method imposes constraints on the way the 7 fields mimicking the SSA22 can be distributed. This restriction makes unable some of the sub-volumes in the box. We decide to keep the number of mock surveys fixed to 15 also for the `random` method in order to allow a fair comparison between the two methods.

2.5   Exploring and selecting good models

We make a thorough exploration of the parameter space for the models $\mathcal{M}$ where $\log_{10} M_{\mathrm{min}}$ takes 30 values from 10.0 up to 12.9 with an even spacing of 0.1 dex. $\log_{10} M_{\mathrm{max}}$ takes values in the same range as $\log_{10} M_{\mathrm{min}}$ only with a displacement of 0.1 dex in the whole range. The occupation fraction f_{occ} takes 10 different values from 0.1 to 1 regularly spaced by 0.1. In total the number of different models $\mathcal{M}$ that are explored is $30 \times 30 \times 10 = 9000$.

The lower limit for the parameter M_{min} is set by the minimum occupation fraction we decide to consider. At $M_{\mathrm{min}} = 10^{10} h^{-1} \mathrm{M}_\odot$ the halo number density around that mass range is ~ 10 times higher than the observational constraints for LAEs. This means that models in that mass range and an occupation fraction $f_{\mathrm{occ}} = 0.1$ have the possibility to be compatible with observations. Lower values for M_{min} require $f_{\mathrm{occ}} < 0.1$, which are not considered in this paper . **In turn exploring occupation fractions on the order of $f_{\mathrm{occ}} = 0.01$ only makes sense for halo populations in the mass range of $10^9 h^{-1} \mathrm{M}_\odot$ which are abundant enough to fit observations with a very low occupation fraction. In our case, this is a mass range unresolved by the Bolshoi simulation and therefore cannot be considered in the present study.**

For each mock survey generated in a given model $\mathcal{M}$ we compute the surface density in its 12 mock fields. We perform a Kolmogorov-Smirnov (KS) to compare these values against the 12 observational values. This tests gives us a value $0 < P < 1$ to reject the null hypothesis, namely that two data sets come from the same distribution. In this paper we consider that for values $P > 0.05$ the two distributions can be thought as coming from the same distribution.

We begin by considering that a model $\mathcal{M}$ with at least one mock survey (out of 15) consistent with observations has viable parameters to host LAEs. From that we consider a stronger constraints to reduce the number of models by asking that all the 15 mocks to be consistent with observations and analyze again the properties of the resulting models. Finally we add the ACF as an additional constraint and consider all the models having their 15 mocks consistent with observations.

The ACF is computed using the Landy & Szalay estimator (Landy & Szalay 1993) on fields of size 1 deg^2 to be compared against the results reported by Ouchi et al. (2010).

The observed and mock ACF are fit to a power-law function:

$$\omega(\theta) = \left(\frac{\theta}{\theta_0} \right)^{-\beta}, \qquad (1)$$

where θ_0 and β are free parameters. The fit is done using a least square minimization procedure. For each mock field we
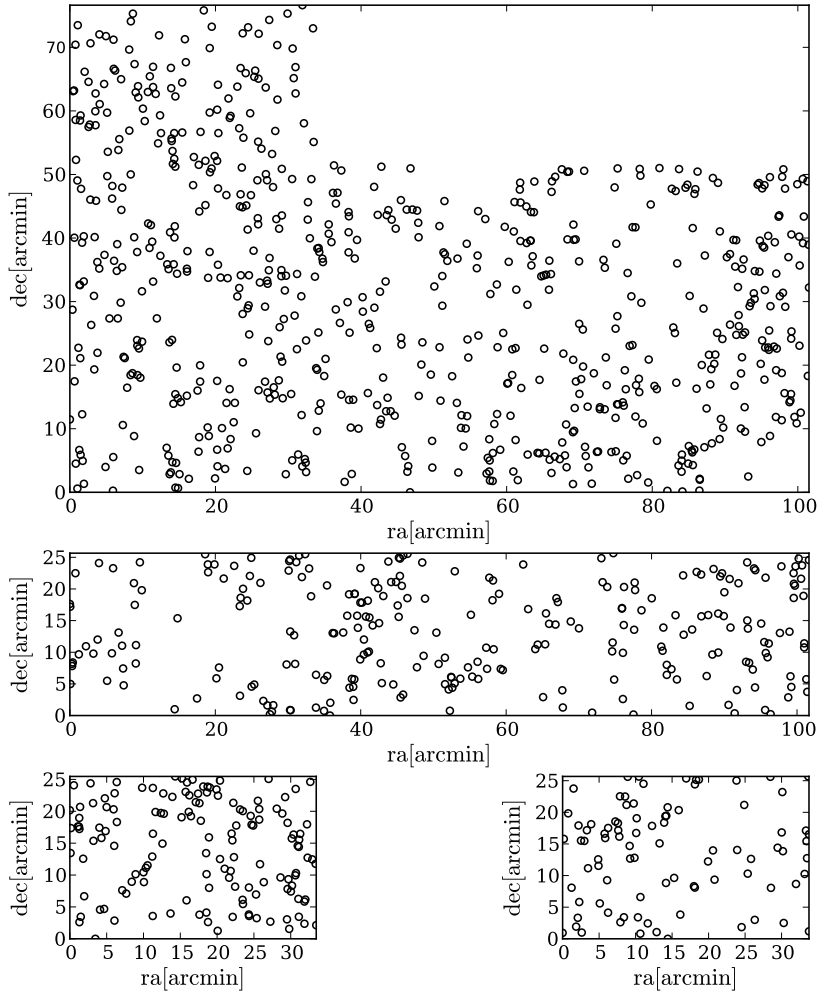
Figure 2. Spatial distribution of a LAEs mock survey for a model with parameters $\log_{10} M_{\min} = 10.4$, $\log_{10} M_{\max} = 10.5$ and $f_{\rm occ} = 0.1$ for the `match` method. The larger panel shows 7 mock fields together mimicking the SSA22 region. The intermediate panel shows 3 mock fields corresponding to the SXDS region. The lower panels represent the SDF and GOODS-North fields. The same model has another 14 associated mock surveys build from different regions in the simulation, but constructed following the same pattern.

obtain a covariance matrix that gives us the uncertainty in the parameters β and θ_0. **We consider that a mock field is consistent with observations if the two parameters β and θ_0 are equal within a 1-σ range.**

3   RESULTS

The main purpose of this section is to show how different observational constraints narrow down the parameters space of allowed models. Each sub-section presents the effect of adding a new piece of observational or statistical evidence.

3.1   Dark Matter Halo Number Density

The right panel in Figure 1 shows the integrated dark matter halo surface density as a function of minimum halo mass $M_{\min}$. Each line corresponds to one of the 210 sub-volumes in the Bolshoi simulation. The gray band indicates the surface density values for LAEs allowed by observations (Yamada et al. 2012). The dashed lines represent the average

values in the fields observed by (Hayashino et al. 2004; Ouchi et al. 2008b).

This plot allows us to understand why only a specific range of models $\mathcal{M}$ can be expected to be consistent with observations. From Figure 1 we can read that models with a minimum mass $M_{\min} > 10^{12} h^{-1} M_\odot$ always have a surface number density lower than the observational constrain, making them incompatible with observations; there are simply too few halos compared to observed LAEs. The opposite is true in models with $M_{\min} < 10^{11.0} h^{-1} M_\odot$ that have a surface number density larger observations. In those cases the maximum mass $M_{\max}$ and the occupation fraction $f_{\rm occ} < 1.0$ can be tuned in order to lower the halo number density to match observations.

Figure 1 also illustrates the impact of cosmic variance. At fixed minimum mass there is an scatter of $0.3-0.6$ dex in the number density abundance, which is of the same order of magnitude as the scatter in the observational data. As a consequence, the variation in the number density in mocks for models with the same mass range and occupation fraction can be by factors of $\sim 2-5$. This scatter induced by

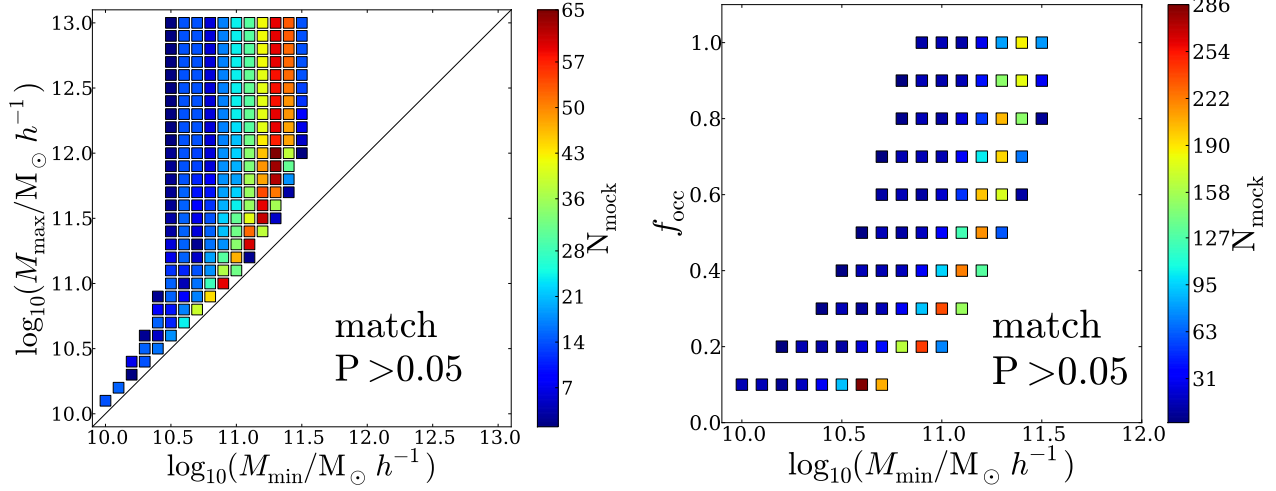**Figure 3.** $M_{\min}$-$M_{\max}$ (left) and $M_{\min}$-f_{occ} (right) planes for all models with KS test values $P > 0.05$. The color code corresponds to the number of mock surveys compatible with observations. Only regions of parameter space with at least one consistent mock survey are included.

cosmic variance is naturally included in the mock construction process. This variance will explain that very different models can be made compatible with observations.

3.2 Models consistent with the surface density distributions

Figure 3 presents regions in parameter space $M_{\min}$-$M_{\max}$, $M_{\min}$-f_{occ} where the KS test between the mocks and observations yields values of $P > 0.05$ for at least one mock survey in each model. For those models it is not possible reject the hypothesis that the simulated and observed data for the surface number density come from the same parent distribution.

In total, there are between 550 to 600 models out of the original 9000 models that have at least one mock survey consistent with observations. By inspection of Figure 3 we see that the halo number abundance is able to constraint the minimum mass $M_{\min}$ to a narrow range, while $M_{\max}$ and f_{occ} remain largely unconstrained.

In Figure 3 there are three regions of parameter space that can be clearly distinguished. The first corresponds to models where the minimum mass is high $M_{\min} > 10^{11.5}h^{-1}\mathrm{M_\odot}$. For these models the number density of LAEs is too low to be compatible with observations.

The second region corresponds to an intermediate range for the minimum mass $10^{10.5}h^{-1}\mathrm{M_\odot} < M_{\min} < 10^{11.5}h^{-1}\mathrm{M_\odot}$ where, regardless of the value of the maximum mass $M_{\max}$, it is possible to tune the occupation fraction f_{occ} to bring some of the mock surveys into good agreement with observations. In this region we find two extreme kinds of models. One extreme are models with a narrow mass interval $\Delta M \equiv \log_{10} M_{\max} - \log_{10} M_{\min} < 1.0$ dex. The other extreme are models with a large mass interval $\Delta M > 1.0$ dex going up to the maximum halo mass present in the simulation at that redshift, with $\Delta M = 2.5$ dex in some cases.

The third region in parameter space corresponds to

$M_{\min} < 10^{10.5}h^{-1}\mathrm{M_\odot}$. In this case only models with a very narrow mass interval of at most 0.5 dex ($M_{\max} < 10^{11.0}h^{-1}\mathrm{M_\odot}$) and low occupation fractions $f_{\mathrm{occ}} \leq 0.3$ are allowed.

Without any additional information our method allows us to infer that most of the successful models are found in the second and third regions of parameter space. This result was expected from halo abundance calculations shown in Figure 1 and discussed in the previous subsection.

However, the additional information we gain with this test is the relative abundance of models in the parameter space. Not all models in the second region have an equal abundance. By inspection of Figure 3 it seems that models with $\log_{10} M_{\min} \sim 10^{11.3}h^{-1}\mathrm{M_\odot}$ and low occupation fraction $f \leq 0.3$ are preferred. In the next sub-sections we explore in detail the models in this region, imposing tighter constraints on the KS test results and exploring the mocks' consistency with the angular correlation function.

3.3 Models with the largest number of consistent mock surveys

In the previous sub-section we use a conservative criterion of agreement by selecting the models that had at least one mock survey with $P > 0.05$ in the KS test. Now we turn to a more strict selection by requiring all the 15 constructed mock surveys to be consistent with observations.

With this cut we find ~ 100 models with all the 15 mock survey realizations with $P > 0.05$. This cut represents a reduction by a factor of ~ 6 with respect to the total number of models with at least one consistent mock.

Figure 4 presents the locii of these models in the parameter space $M_{\min} - M_{\max}$ and $M_{\min} - f_{\mathrm{occ}}$. With this constraint the number of consistent models with $10.5 < \log_{10} M_{\min} < 11.0$ are reduced. This corresponds to the regions in the parameter space in Figure 3 that already had a low number of consistent mock surveys. On the other hand,
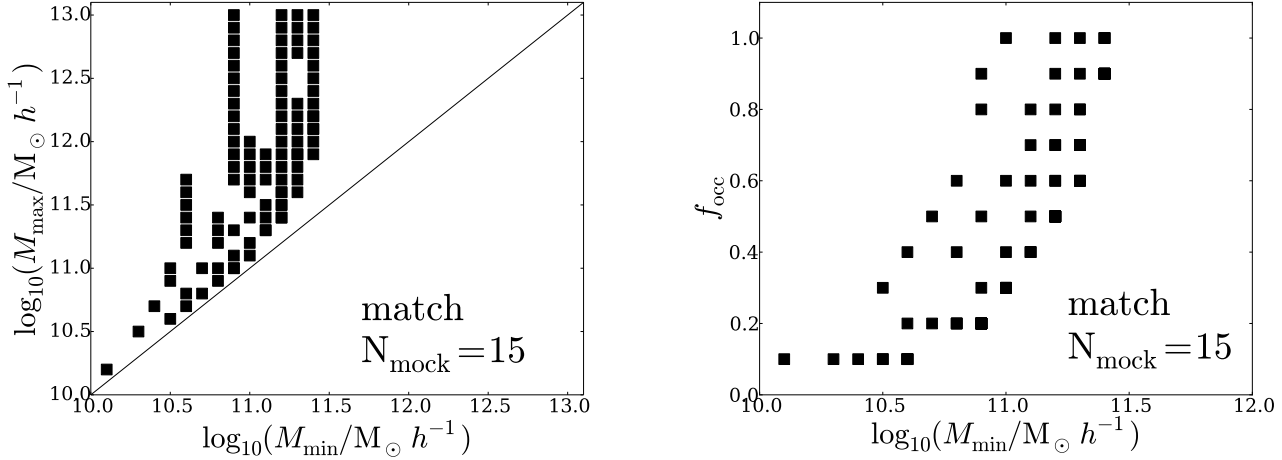
Figure 4. Favored regions in parameter space when the constraints on the maximal number of consistent mocks is imposed. Only the results for the `match` method are shown.

from the right panel in Figure 4 we see that the favored occupation fraction still remain unconstrained $0 \leq f_{\mathrm{occ}} \leq 1.0$.

We conclude that conditions on the number density statistics, even if they are very strict, only put strong constraints on the minimum mass M_{min} but not on the other two parameter of the model M_{max} and f_{occ}.

3.4 Consistency with the Angular Correlation Function

Figure 5 shows the results for the best estimates of θ_0-β used in the ACF parameterization. Blue circles with error bars represent the results from the mocks and the horizontal line the observational results of Ouchi et al. (2010) over a field with average number density where the β parameter was fixed in the fit. From this Figure we observe that there are models with too large values of θ_0 and β that can be ruled out as inconsistent with the angular correlation function.

Figure 6 presents the remaining consistent models in the planes M_{min}-M_{max} and M_{min}-f_{occ}. A model is consistent with observations if there is a 1-σ overlap between both the correlation length θ_0 and the exponent β. We find that we end up with 40 models consistent with the ACF constraints.

Comparing Figure 6 with Figure 4 we see that the new constraint disfavors almost all models with $M_{\mathrm{max}} > 10^{12}$. The only exception is a narrow range of models with $M_{\mathrm{min}} = 10^{10.9}$. However, we have verified that these models are only marginally consistent with the ACF constraints in the θ_0-β plane.

From this comparison we conclude that clustering information can constraint the values of M_{max}, but not the occupation fraction.

4 DISCUSSION

Out of the initial set of 9000 models we end up with 40 that are consistent with the observational constraints. To facilitate the discussion of these models we define a new quantity, the halo mass range $\Delta M = \log_{10} M_{\mathrm{max}} - \log_{10} M_{\mathrm{min}}$,
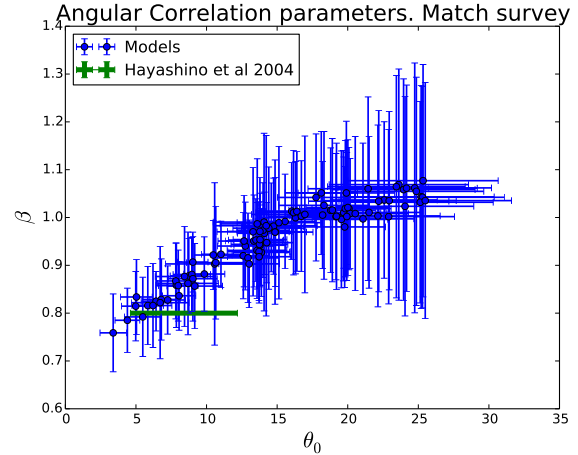

Figure 5. Values for the free parameters θ_0 and β in the fitting formula (Eq. 1) for the angular correlation function. Blue dots correspond to simulations and the green line to observations by Ouchi et al. (2010). The error bars in the theoretical data correspond to the quadratic average of the fitting errors for each mock survey

which together with the occupation fraction, f_{occ}, and the minimum mass M_{min} allows us to classify all the successful models into three families:

(1) Low occupation fraction $f_{\mathrm{occ}} \leq 0.2$ and narrow mass range $\Delta M \leq 1.0$ dex: 16 models.
(2) High occupation fraction $f_{\mathrm{occ}} > 0.2$ and narrow mass range $\Delta M \leq 1.0$: 17 models
(3) Low occupation fraction $f_{\mathrm{occ}} \leq 0.2$ and wide mass range $\Delta M > 1.0$: 7 models

A complete parameter list for the three families is presented in Tables 1, 2 and 3.

The models in the third family are barely consistent with the constraints from the ACF. They have mean values of θ_0 outside the observational uncer-
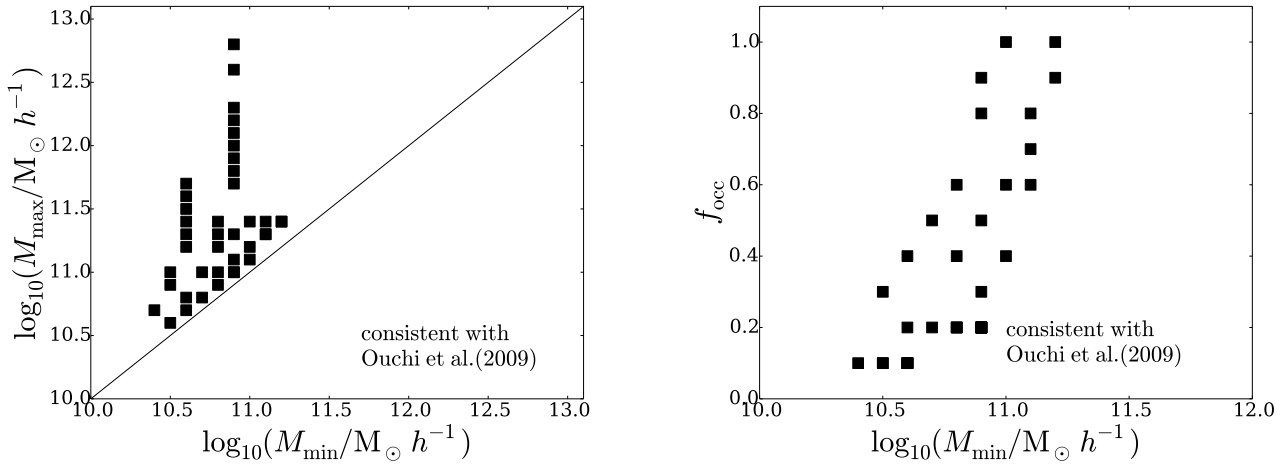
Figure 6. Planes $M_{\min}$-$M_{\max}$ (left) and $M_{\min}$-f_{occ} (right). with the models fulfilling both constraints on the maximal number of consistent mocks and the angular correlation function. The observational data corresponds to Ouchi et al. (2010).

tainties, but have are considered as consistent because their large error bars overlap. These models they have another particular feature: their minimum mass is exactly $M_{\min} = 10^{10.9} h^{-1} \mathrm{M}_\odot$. Because these models are are barely compatible with observations and are a minority of the consistent models, we exclude them from the rest of the discussion.

4.1 Two relevant features

There are two interesting features in the remaining two first families. First, the occupation fraction can take any value from 0.1 to 1.0. Second, the halos hosting LAEs all have a narrow mass range $\Delta M \leq 1.0$.

The existence of models with high occupation fractions $f_{\mathrm{occ}} > 0.2$ is unexpected from previous clustering analysis that do not take account the effect of cosmic variance in the same way we propose in this paper . Nevertheless, the mass range predicted by our models is consistent with already published observational results. This suggests that taking explicitly cosmic variance into account hinders the possibility of constraining the LAEs occupation fraction.

Concerning the narrow mass range $\Delta M < 1.0$ the question arises of how can we give a physical interpretation for the existence of such a narrow mass range. We can start with a reasonable assumption. Namely that star formation rate increases with halo's mass.

Under this assumption the cut at the low mass end, $M_{\min}$, can be interpreted in terms of the minimal star formation rate required to produce a Lyα luminosity above observational detection thresholds. A cut at higher halo masses $M_{\max}$ requires a different justification. There are two complementary physical scenarios that could provide

One scenario can be presented in terms of a decreasing escape fraction of Lyα radiation in massive systems. Detailed galaxy formation models support the idea that massive galaxies with higher metallicities have larger dust contents and a less concentrated ISM than lower mass systems.

Due to the resonant nature of the Lyα line the probability of absorption of Lyα photons increases in massive systems, producing high absorption of the Lyα line but not of UV continuum or other non-resonant lines (Laursen et al. 2009; Forero-Romero et al. 2011). In a second scenario larger systems have more extended gaseous envelopes which due to resonance effects of the Lyα line, induces a low surface brightness and a broader line, making these systems less observable in narrow band filter surveys (Laursen et al. 2009; Zheng et al. 2010).

4.2 Comparison to other clustering estimates

Observational evidence based on the ACF inferred from photometric measurements in the Extended Chandra Deep Field South has shown that the median dark matter masses of halos hosting LAEs is $\log_{10} M_{\mathrm{med}} = 10.9^{+0.5}_{-0.9} \mathrm{M}_\odot$, with a corresponding occupation fraction of $1-10\%$ (Gawiser et al. 2007). Ouchi et al. (2010) presents analysis of LAE observations in the redshift interval $3.1 < z < 7.0$ and at $z = 3.1$ They quote an average mass for the host dark matter halos of $M_h = 2.9^{+24.0}_{-2.9} \times 10^{10}\ h^{-1} \mathrm{M}_\odot$ with a corresponding duty cycle of 0.008 ± 0.03.

Our results are in a general good agreement with those estimates for the host mass. This is not completely unexpected given that we have also required consistency with ACF measurements. These expectations are **mostly** matched by the first family of models, also summarized in Table 1. These models, which favor only the low occupations fractions, are also consistent in that regards with the observational expectations.

The novelty in our results is that we have a detailed estimate for host halo mass range together with the escape fraction. This allows us to show that the halo mass range can, in some cases, be narrow $\Delta M < 0.3$dex, something that cannot be inferred from ACF analysis alone. Furthermore, In contrast to (Gawiser et al. 2007) and (Ouchi et al. 2010) we find that an ACF analysis on a single data-set is not enough to rule out models with a high occupation fraction $f_{\mathrm{occ}} > 0.3$, which represent half of our best models.

$\log_{10} M_{\min}$	$\log_{10} M_{\max}$	$f_{\rm occ}$	ΔM
10.4	10.7	0.1	0.3
10.5	10.9	0.1	0.4
10.5	11.0	0.1	0.5
10.6	10.8	0.2	0.2
10.6	11.2	0.1	0.6
10.6	11.3	0.1	0.7
10.6	11.4	0.1	0.8
10.6	11.5	0.1	0.9
10.6	11.6	0.1	1
10.7	11.0	0.2	0.3
10.8	11.2	0.2	0.4
10.8	11.3	0.2	0.5
10.8	11.4	0.2	0.6
10.9	11.9	0.2	1.0
10.9	11.7	0.2	0.8
10.9	11.8	0.2	0.9

Table 1. List of parameters for the first family of models. Narrow mass range $\Delta M \leq 1.0$ dex and low occupation fraction $f_{\rm occ} \leq 0.3$.

$\log_{10} M_{\min}$	$\log_{10} M_{\max}$	$f_{\rm occ}$	ΔM
10.5	10.6	0.3	0.1
10.6	10.7	0.4	0.1
10.7	10.8	0.5	0.1
10.8	10.9	0.6	0.1
10.8	11.0	0.4	0.2
10.9	11.0	0.8	0.1
10.9	11.0	0.9	0.1
10.9	11.1	0.5	0.2
10.9	11.3	0.3	0.4
11.0	11.1	1.0	0.1
11.0	11.2	0.6	0.2
11.0	11.4	0.4	0.4
11.1	11.3	0.7	0.2
11.1	11.3	0.8	0.2
11.1	11.4	0.6	0.3
11.2	11.4	0.9	0.2
11.2	11.4	1.0	0.2

Table 2. List of parameters for the second family of models. Narrow mass range $\Delta M \leq 0.4$ dex and high occupation fraction $f_{\rm occ} > 0.2$.

$\log_{10} M_{\min}$	$\log_{10} M_{\max}$	$f_{\rm occ}$	ΔM
10.6	11.7	0.1	1.1
10.9	12.0	0.2	1.1
10.9	12.1	0.2	1.2
10.9	12.2	0.2	1.3
10.9	12.3	0.2	1.4
10.9	12.6	0.2	1.7
10.9	12.8	0.2	1.9

Table 3. List of parameters for the third family of models. Wide mass range $\Delta M > 1.0$ dex and low occupation fraction $f_{\rm occ} \leq 0.2$. **These models are barely consistent with the constraints from the Angular Correlation Function and have been excluded from the main discussion.**

4.3 In the context of abundance matching models

The abundance matching methods are based on observational results for Lyman Break Galaxies (LBGs) (Behroozi et al. 2013b,a). In the case of Behroozi et al. (2013b) the minimum halo mass considered to be relevant in their analysis is $10^{11.4} h^{-1} M_\odot$. They report stellar mass mass around $(1.0 \pm 0.3) \times 10^{9.0}\ h^{-1} M_\odot$, while their star formation rate is in the range $0.6 \pm 0.2\ M_\odot {\rm yr}^{-1}$, which nevertheless are close to the lower bound of values inferred for LAEs at high redshift (Gawiser et al. 2007; Nilsson et al. 2009; Pentericci et al. 2009).

In our results, all the preferred models have a halo mass range lower than the minimum of $M_{\min} < 10^{11.4} h^{-1} M_\odot$ considered in abundance matching at $z = 3$. Our results confirm the expectations that most of LAEs are to be found in less massive halos LBG hosts. A detailed analysis of the spectral and photometric properties of LAEs coupled to the kind of analysis performed in this paper can be a guide in the study of the properties of low mass dark matter halos at $z = 3.1$, extending the capabilities of abundance matching methods.

4.4 Caveats of our method

There are two important caveats for the work presented here. The first is the assumption of a single LAE per dark matter halo. This contradicts the general expectation of dark matter sub-halos in the simulation to host satellite galaxies. However, it has been found in analysis based on the shape of the correlation function (Jose et al. 2013) that satellite galaxies are not a dominant population, making our initial approximation a reasonable one. **The lack of close pairs** Therefore we conclude that including the effect of satellite galaxies does not change the main results reported in this paper .

The second caveat are the precise values for the mass intervals. These values are quoted from halos defined using a FOF halo finder. Different halo finders and definitions for the detection density threshold can yield different masses up to a factor ~ 2(More et al. 2011). For instance a Friends-of-Friends algorithm with linking length $l = 0.20$ times the average inter-particle distance finds halos on average 1.4 times less massive than halos defined with an spherical overdensity algorithm halos (Klypin et al. 2011). Therefore, the mass values for $M_{\min}$ and $M_{\max}$ should not be considered exact within less than ~ 0.2 dex.

Turning filter values into cosmological volumes.

Comparing results for the clustering and the ACF from surveys with different EW cuts.

4.5 On the reproducibility of our results

All the software, raw and processed data to produce the results and plots in this paper are publicly available in a github repository [2]. Most of the code to produce the plots can be found as an Ipython notebook (Pérez & Granger 2007) in the same repository.

---

[2] https://github.com/forero/CosmicVarianceLAES

5   CONCLUSIONS

In this paper we look for constraints on the preferred mass and occupation fraction of dark matter halos hosting Lyman Alpha Emitters at redshift $z = 3.1$ in a ΛCDM cosmology. We perform this study paying special attention to the impact of cosmic variance on these results. To this end we build a large number of mock catalogs matching observational geometries. The mocks are constructed from a N-body simulation following a simple recipe to assign a single LAE to each halo. Only a fraction $f_{\rm occ}$ of halos within a mass range $M_{\rm min} < M_{\rm h} < M_{\rm max}$ can host a LAE.

We then proceed with a thorough exploration of the space of free parameters $M_{\rm min}$, $M_{\rm max}$ and $f_{\rm occ}$ to find mocks that are consistent with two observational constraints: the surface number density and the angular correlation function. Out of the initial 9000 combinations of parameters in the model we find 40 combination of parameters consistent with observations.

We find that **the information for the number density constrains the minium mass to the range $10^{10}h^{-1}{\rm M}_\odot < M_{\rm min} < 10^{11.5}h^{-1}{\rm M}_\odot$ while the clustering constrains the upper mass $M_{\rm max} < 10^{12}h^{-1}{\rm M}_\odot$. However, this is insufficient to impose a tight constraint on the escape fraction.** Furthermore, we find that the mass range defined as $\Delta M = \log_{10} M_{\rm max} - \log_{10} M_{\rm min}$ is always $\Delta M \leq 1.0$.

The wide range in values for the escape fraction is allowed by the large dispersion in the statistics derived from the mocks. This uncertainty is unexpected from previous studies that unanimously favor low values for the occupation fractions (i.e. Gawiser et al. 2007; Ouchi et al. 2010). Nevertheless, all the halo mass ranges and occupation fractions deduced previous analysis are a subset of the models we find in this paper .

All of our preferred models support the notion that the most massive halos at $z = 3.1$ do not host detectable LAEs. The existence of a narrow mass range for halos hosting LAEs, $\Delta M \leq 1.0$ dex, has two different explanations at least. The first is having LAEs with a decreasing Lyα escape fraction with increasing mass, the second is having larger screening effects by neutral Hydrogen around the most massive systems (Laursen et al. 2009; Forero-Romero et al. 2011).

We also find extreme cases with a very narrow $\Delta M < 0.3$, meaning that there is barely a factor of ~ 2 between the minimum and halo mass. If these models can be confirmed, it would mean a great challenge for galaxy formation models to explain how is that LAEs can be hosted in such a narrow range of halo mass.

In summary, we show that **the currently available spatial information of LAEs cannot put a tight constraint on their occupation fraction of dark matter halos**. This information can confidently be used to establish that these galaxies are hosted in low mass halos with masses within a range spanning less than a factor of ten. We foresee that the new observations with new instruments (such as MUSE, Hyper SuprimeCam and HETDEX) covering larger fields and a wider range of luminosities will be key in reducing cosmic variance and imposing tighter constraints on the properties of dark matter halos hosting LAEs. At the same time, additional modeling for Lyα radiation transfer is needed to put a tighter constrain on the Lyα escape fraction in high redshift galaxies, also paying attention to newly framed physical phenomena, such as the stochasticity (Forero-Romero & Dijkstra 2013) in the star formation process, which might play a role in inducing detection biases in high redshift LAEs.

REFERENCES

Behroozi P. S., Wechsler R. H., Conroy C., 2013a, ApJL, 762, L31

Behroozi P. S., Wechsler R. H., Conroy C., 2013b, ApJ, 770, 57

Colberg J. M., White S. D. M., Yoshida N., MacFarland T. J., Jenkins A., Frenk C. S., Pearce F. R., Evrard A. E., Couchman H. M. P., Efstathiou G., Peacock J. A., Thomas P. A., Virgo Consortium 2000, MNRAS, 319, 209

Dayal P., Ferrara A., Saro A., Salvaterra R., Borgani S., Tornatore L., 2009, MNRAS, 400, 2000

Dijkstra M., Kramer R., 2012, MNRAS, 424, 1672

Dijkstra M., Mesinger A., Wyithe J. S. B., 2011, MNRAS, 414, 2139

Forero-Romero J. E., Dijkstra M., 2013, MNRAS, 428, 2163

Forero-Romero J. E., Yepes G., Gottlöber S., Knollmann S. R., Cuesta A. J., Prada F., 2011, MNRAS, 415, 3666

Forero-Romero J. E., Yepes G., Gottlöber S., Prada F., 2012, MNRAS, 419, 952

Garel T., Blaizot J., Guiderdoni B., Schaerer D., Verhamme A., Hayes M., 2012, MNRAS, 422, 310

Gawiser E., Francke H., Lai K., Schawinski K., Gronwall C., Ciardullo R., Quadri R., Orsi A., Barrientos L. F., Blanc G. A., Fazio G., Feldmeier J. J., 2007, ApJ, 671, 278

Gawiser E., Francke H., Lai K., Schawinski K., Gronwall C., Ciardullo R., Quadri R., Orsi A., Barrientos L. F., Blanc G. A., Fazio G., Feldmeier J. J., Huang J.-s., Infante L., Lira P., Padilla N., 2007, ApJ, 671, 278

Guaita L., Francke H., Gawiser E., Bauer F. E., Hayes M., Östlin G., Padilla N., 2013, A&A, 551, A93

Hayashino T., Matsuda Y., Tamura H., Yamauchi R., Yamada T., Ajiki M., Fujita S. S., Murayama T., Nagao T., Ohta K., Okamura S., Ouchi M., Shimasaku K., Shioya Y., Taniguchi Y., 2004, AJ, 128, 2073

Jarosik N., Bennett C. L., Dunkley J., Gold B., Greason M. R., Halpern M., Hill R. S., Hinshaw G., Kogut A., Komatsu E., Larson D., Limon M., 2011, ApJS, 192, 14

Jose C., Srianand R., Subramanian K., 2013, ArXiv e-prints

Klypin A. A., Trujillo-Gomez S., Primack J., 2011, ApJ, 740, 102

Koehler R. S., Schuecker P., Gebhardt K., 2007, A&A, 462, 7

Komatsu E., Dunkley J., Nolta M. R., Bennett C. L., Gold B., Hinshaw G., Jarosik N., Larson D., Limon M., Page L., Spergel D. N., Halpern M., 2009, ApJS, 180, 330

Kudritzki R.-P., Méndez R. H., Feldmeier J. J., Ciardullo R., Jacoby G. H., Freeman K. C., Arnaboldi M., Capaccioli M., Gerhard O., Ford H. C., 2000, ApJ, 536, 19

Landy S. D., Szalay A. S., 1993, ApJ, 412, 64

Laursen P., Duval F., Östlin G., 2013, ApJ, 766, 124

Laursen P., Razoumov A. O., Sommer-Larsen J., 2009, ApJ, 696, 853

Laursen P., Sommer-Larsen J., 2007, ApJL, 657, L69

Matsuda Y., Yamada T., Hayashino T., Tamura H., Yamauchi R., Murayama T., Nagao T., Ohta K., Okamura S., Ouchi M., Shimasaku K., Shioya Y., Taniguchi Y., 2005, ApJL, 634, L125

More S., Kravtsov A. V., Dalal N., Gottlöber S., 2011, ApJS, 195, 4

Neufeld D. A., 1991, ApJL, 370, L85

Nilsson K. K., Møller P., Möller O., Fynbo J. P. U., Michałowski M. J., Watson D., Ledoux C., Rosati P., Pedersen K., Grove L. F., 2007, A&A, 471, 71

Nilsson K. K., Tapken C., Møller P., Freudling W., Fynbo J. P. U., Meisenheimer K., Laursen P., Östlin G., 2009, A&A, 498, 13

Orsi A., Lacey C. G., Baugh C. M., 2012, MNRAS, 425, 87

Ouchi M., Shimasaku K., Akiyama M., Simpson C., Saito T., Ueda Y., Furusawa H., Sekiguchi K., Yamada T., Kodama T., Kashikawa N., Okamura S., Iye M., Takata T., Yoshida M., Yoshida M., 2008a, ApJS, 176, 301

Ouchi M., Shimasaku K., Akiyama M., Simpson C., Saito T., Ueda Y., Furusawa H., Sekiguchi K., Yamada T., Kodama T., Kashikawa N., Okamura S., Iye M., Takata T., Yoshida M., Yoshida M., 2008b, ApJS, 176, 301

Ouchi M., Shimasaku K., Furusawa H., Saito T., Yoshida M., Akiyama M., Ono Y., Yamada T., Ota K., Kashikawa N., Iye M., Kodama T., Okamura S., Simpson C., Yoshida M., 2010, ApJ, 723, 869

Peebles P. J. E., 1980, The large-scale structure of the universe

Pentericci L., Grazian A., Fontana A., Castellano M., Giallongo E., Salimbeni S., Santini P., 2009, A&A, 494, 553

Pérez F., Granger B. E., 2007, Comput. Sci. Eng., 9, 21

Riebe K., Partl A. M., Enke H., Forero-Romero J., Gottlber S., Klypin A., Lemson G., Prada F., Primack J. R., Steinmetz M., Turchaninov V., 2013, Astronomische Nachrichten, 334, 691

Springel V., White S. D. M., Jenkins A., Frenk C. S., Yoshida N., Gao L., Navarro J., Thacker R., Croton D., Helly J., Peacock J. A., Cole S., Thomas P., Couchman

H., Evrard A., Colberg J., Pearce F., 2005, Nature, 435, 629

Verhamme A., Schaerer D., Maselli A., 2006, A&A, 460, 397

Walker-Soler J. P., Gawiser E., Bond N. A., Padilla N., Francke H., 2012, ApJ, 752, 160

Yajima H., Choi J.-H., Nagamine K., 2012, MNRAS, 427, 2889

Yamada T., Nakamura Y., Matsuda Y., Hayashino T., Yamauchi R., Morimoto N., Kousai K., Umemura M., 2012, AJ, 143, 79

Zheng Z., Cen R., Trac H., Miralda-Escudé J., 2010, ApJ, 716, 574